Experimental study of the influence of the swirl number on lean premixed combustion regimes

Letícia Carneiro Piton, Gabriela Senra Pessanha Rios Nobrega, Luís Fernando Figueira da Silva, Philippe Scouflaire, Nasser Darabiha

Noname manuscript No.
(will be inserted by the editor)

Experimental study of the influence of the swirl number on lean premixed combustion regimes

Letícia Carneiro Piton · Gabriela Senra Pessanha Rios Nobrega · Luís Fernando Figueira da Silva · Philippe Scouflaire · Nasser Darabiha

Received: date / Accepted: date

Abstract Lean premixed turbulent swirling combustion is known for significantly reducing pollutants emissions, when compared to non-premixed turbulent flames. Characterizing the swirl number influence is therefore essential to comparing different combustion chamber operational regimes. The present study is devoted to the experimental characterization of a new family of swirlers currently being developed. The associated combustion process is found to exhibit different flame topologies, or combustion regimes, which are functions of the mixture equivalence ratio and flow rate. The flame topologies and the boundaries between the observed combustion regimes are evidenced by means of OH^* chemiluminescence and overall flame chemiluminescence.

Keywords experimental study · swirling flows · flame topology · premixed turbulent flames

1 Introduction

Lean premixed turbulent combustion is known for significantly reducing pollutants emissions when compared to non-premixed turbulent flames. These premixed flames are often considered in swirling combustion chamber configurations, where the swirl number influence has been shown to be paramount on controlling turbulent flame topologies, blow-off or flashback limits and on the acoustic stability properties [4, 6, 10]. Characterizing the swirl number influence is therefore essential to comparing different combustion chamber operational regimes. Such comparison is particularly relevant when novel swirler designs are sought, which is the case of the present endeavor.

Letícia Carneiro Piton
Pontifícia Universidade Católica do Rio de Janeiro, Brazil
Tel.: +33 06 03 80 42 16
E-mail: leticia.carneiro-piton@cnrs-orleans.fr
Present address: Laboratoire ICARE, CNRS Orléans, France

This study is devoted to the experimental characterization of a new family of swirlers currently being developed in a partnership between PUC-Rio and EM2C/CNRS laboratory at CentraleSupelec [21]. The swirl number is classically defined as the ratio between the axial flux of tangential momentum and the axial momentum flux. The considered radial swirlers are characterized by different feed orifices diameters, numbers and angles, and also by variations on the central inverted cone bluff-body position. It should be noted that the present work is a first step towards a more comprehensive experimental study involving velocity and species measurements.

Several recent numerical studies on lean premixed turbulent swirl stabilized combustion have been performed. Using large eddy simulation (LES), previous studies have determined how minute vane modification on a radial swirler impacts both the average velocity distribution and the unsteady flow structures, such as the classical precessing vortex core found on such swirling configurations [2]. The unsteady flowfield structure and corresponding flame topologies has been shown to be influenced by the combustion chamber wall temperature, in studies which also considered radial swirlers [15]. Comparisons between experimental and LES isothermal and reactive flowfields have also been performed [16] on radial swirling combustion chambers, with emphasis on the role played by the outlet contraction. Axial swirling lean premixed turbulent combustion has been studied, comparing the LES velocity fields and flame topologies to those experimentally measured [6]. In that work, a dynamic sub-filter model has been used to describe the momentum transport, whereas combustion is modeled using an artificially thickened flame approach and a reduced chemistry mechanism. Fluid swirl number measurements has been shown to exhibit significant discrepancies with respect to the geometrical swirl number, which may be determined based on a formal order of magnitude analysis from the relevant geometrical features [8,7].

Experimental studies have been devoted to developing a combustor blow-off model, which is based on the computed adiabatic flame temperature and the associated effect on the extinction strain rate of laminar premixed flames [1]. Even if the fluid dynamics time scale is assumed invariant in that work, the measured blow-off velocity evolution with mixture equivalence ratio is captured by the model. Using a combination of an axial swirler and a bluff-body somewhat similar those developed in the present study, it has been demonstrated that a blow-off Damköhler number could be expressed for the different studied flames as a function of the combustor power [5]. This Damköhler number was defined as the square root of the ratio between the bulk flow and the unstretched laminar premixed flame time scales. More recently, it has been evidenced how the natural gas combustion blow-off and flash-back diagrams are influenced both by the swirl number and by the $O_2/N_2/CO_2$ content in the combustible mixture [11]. For a given total mass flow rate, increasing either the swirl number or the oxygen content allows an ampler operational range, in terms of equivalence ratio or heat input. The combustion chamber geometry has been found to modify the methane-air blow-off limit [24]. Indeed, for a given mass flow rate and swirl number, a circular cross-section combustor led

to smaller blow-off equivalence ratio compared to a rectangular one. Premixed turbulent swirling flames of different $O_2/N_2/CO_2$ and CH_4 contents have been compared [12], evidencing that the swirl number, the adiabatic flame temperature and the ratio between the flow bulk velocity exert a controlling effect on the flame shape and position. For the studied equivalence ratios and CO_2 dilutions, flame shape transition occurred always at the same swirl number value. The mechanisms controlling some of the flame shape transitions have been associated to the ratio between a recirculation zone characteristic frequency and the premixed flame extinction strain rate [26,22]. Furthermore, this frequency has been shown to be Reynolds number independent, and to be a linear function of the inlet flow bulk velocity, leading to a constant Strouhal number.

The above cited studies indicate that the different combustion regimes found in turbulent premixed swirling combustors are influenced by the swirl number, the Reynolds number, the mixture composition (via the adiabatic flame temperature), and a Damköhler number. The objective of this paper is thus to determine the boundaries between the different combustion regimes characteristic of a novel swirler configuration [21]. This characterization is performed here by means of OH^* chemiluminescence and overall flame chemiluminescence.

2 Experimental Methodology

2.1 Combustion chamber and swirlers

One of the considered swirlers in this paper is shown in Fig. 1(a) as a typical example. The gas mixture is fed to the chamber through the orifices which are offset with respect to the main swirler axis. The orifices are tangent to the 10 mm diameter swirling chamber walls, which length is 33 mm. The central part of this chamber is occupied by a 4 mm diameter cylinder, which is topped by an inverted cone that has a base diameter of 8 mm. This cone base acts as a flame stabilizing bluff-body.

Figure 1(b) presents the combustion chamber. The methane/air mixture is introduced through a convergent located upstream to the swirlers (not shown). The combustion chamber is limited by a confinement placed at the top of the burner, shown in Fig. 2. The confinement consists of a stainless steel base and four quartz windows of 10 mm thickness and 170 mm height. Cooling water flows through the steel base.

The power of the burner, calculated as $P = \dot{m} \cdot LHV$, where $\dot{m}$ is the mass flow rate and LHV is the lower heating value of methane, and is found to vary between 0.5 and 3.6 kW in this study. The Reynolds number (Re) is estimated at two different sections: at the flow inlet (orifices) and at the flow outlet (bluff-body). The characteristic diameter used for calculating Re at the inlet is the orifice diameter, d multiplied by the number of orifices, n. The characteristic diameter of the flow outlet is the hydraulic diameter of the cone

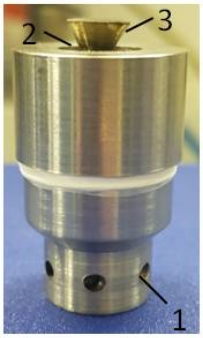

(a) Swirler: 1 - air/fuel inlet orifices, 2 - flow outlet area, 3 - bluff-body.

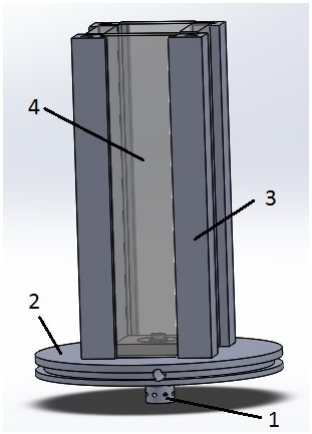

(b) Combustion Chamber: 1 - swirler, 2 - cooling base, 3 - confinement, 4 - quartz window.

Fig. 1 Typical swirler and combustion chamber.

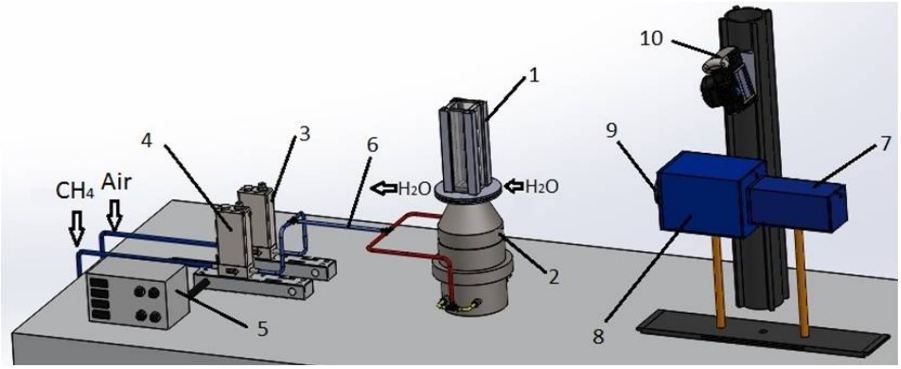

Fig. 2 Experimental test bench scheme: 1 - combustion chamber, 2 - burner, 3 - air flowmeter, 4 - methane flowmeter, 5 - flowmeter controller, 6 - mixture pipe, 7 - CCD camera, 8 - image intensifier IRO, 9 - 310 nm filter, 10 - Canon camera.

trunk of the bluff-body:

$$Re_{in} = \frac{4\dot{\forall}}{\nu n \pi d}; \quad Re_{out} = \frac{4\dot{\forall}}{\nu(D - D_b)}, \tag{1}$$

where ν is the mixture kinematic viscosity, D is the inner diameter of the swirler, D_b is the diameter of the inverted cone base and $\dot{\forall}$ is the volume flow rate. The corresponding values are determined to span from 2.1×10^3 to 7.4×10^3 (Re_{in}) and from 5.1×10^4 to 1.4×10^5 (Re_{out}).

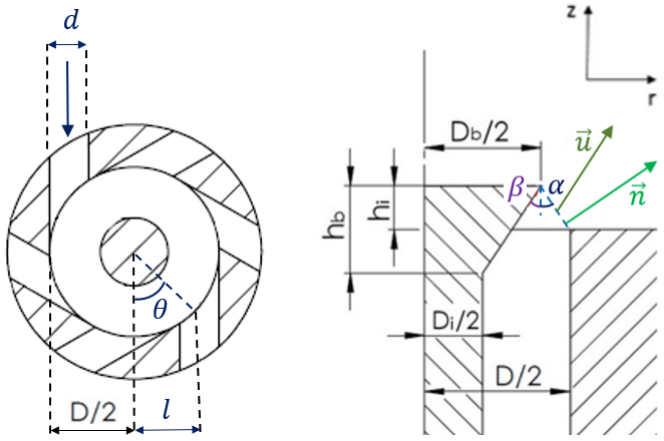

Fig. 3 Swirler intlet (left) and exit (right) planes.

2.2 Swirl number

The swirl number (S) characterizes the swirl intensity and is defined as the ratio between the axial flux of tangential momentum, G_θ, and the axial momentum flux, G_z. Indeed, assuming that the fluid performs a solid body rotation in the swirler [7], $u_\theta(r) = \Omega r$, that the axial velocity component (u_z) is uniform, and ignoring the pressure effects, the swirl number may be expressed as:

$$S = \frac{G_\theta}{RG_z} = \frac{\int_0^R u_z u_\theta r^2 dr}{R\int_0^R u_z^2 r dr} = \frac{1}{2}\frac{u_\theta(R)}{u_z}, \tag{2}$$

in which R is the swirler radius.

Considering the mass conservation in the tubes and the geometry of the exit section shown in Fig. 3, it is possible to determine $u_\theta(R)$ as

$$u_\theta = \dot{\forall}\frac{4}{\pi n d^2}\sin\theta, \tag{3}$$

where $\sin\theta = \frac{l}{D/2}$.

To determine u_z, it is assumed that the velocity vector is parallel to the inverted cone surface at the exit plane. Thus, considering the geometry shown in Fig. 3, the volume flux at this plane allows to write

$$\dot{\forall} = u_z A_z \left(1 + \frac{\tan\beta}{\tan\alpha}\right). \tag{4}$$

$$\tan\beta = \frac{D_b - D_i}{2h_b}; \quad \tan\alpha = \frac{D - D_b}{2h_i}. \tag{5}$$

in which D_i is the diameter of the inner cylinder, h_i is the clearance between the bluff-body top surface and the swirler exit and h_b is the height of the inverted cone base. Replacing these expressions in Eq. (5) one can write

Table 1 Geometrical features and swirl number of the swirler configurations.

	n	d	h_i	h_b	S
SW08a	8	2.5	3	3	1.4
SW08b	8	2.5	0	3	0.9
SW05	5	2	3	3	1.3

$$\frac{1}{u_z} = \frac{\pi D^2}{4\dot{\forall}} \left[1 - \frac{D_b}{D}^2\right] \left[1 + \frac{D_b - D_i}{D - D_b} \frac{h_i}{h_b}\right]. \tag{6}$$

Finally, the swirl number can be expressed as

$$S = \underbrace{\frac{lD}{nd^2}}_{(a)} \underbrace{\left[1 - \left(\frac{D_b}{D}\right)^2\right]}_{(b)} \underbrace{\left[1 + \frac{D_b - D_i}{D - D_b} \frac{h_i}{h_b}\right]}_{(c)}. \tag{7}$$

Equation (7) represents the combination of an usual swirl number expression (a), the influence of the central cylinder (b) and the combined effect of the bluff-body angle and height (c), thus showing how the geometry of the swirler influences the swirl number.

In order to analyze different regions of confined flames, a preliminary study was performed using three swirlers, one of which, SW08a, is shown in Fig. 1(b). This swirler and SW08b differ on the bluff-body height only, and thus on the swirling chamber outlet area. Both these models have 8 orifices, each with a 2.0 mm diameter, so the swiling chamber inlet area is 25.13 mm^2. On the other hand, SW05 has only 5 orifices, each with 2.5 mm diameter, therefore with a 24.54 mm^2 of inlet area, i.e., slightly smaller than SW08.

Table 1 summarizes the geometrical parameters of each studied swirler, along with the geometrical swirl number for each design at the last column. This table illustrates that it is possible to obtain similar S values with distinct swirl geometrical parameters. For this reason, only SW08a and SW08b are compared on the results, which are further discussed in section 3.2.

2.3 Experimental setup

Figure 2 shows the experimental test bench which is composed of the burner, the combustion chamber, the convergent, two flow meters for air, a flow controller for methane, a CCD camera (Imager Intense, LaVision) with an intensifier (Intensified Relay Optics, LaVision) and a Canon (EOS Rebel T5) camera.

The flow meter used for methane is a Bronkhorst mass flow controller (series F-201AC) with a maximum range of 138.9 cm^3/s with 0.5 % reading plus 0.1 % full scale uncertainty. The air volumetric flow rate is measured using a pair of rotameters (Omega, 4T70903X12 and 4T708TX12 models),

Table 2 Equivalence ratios considered and corresponding absolute and relative uncertainties.

	SW08a		SW08b	
ϕ	U_ϕ	U_ϕ/ϕ (%)	U_ϕ	U_ϕ/ϕ (%)
0.39	-	-	0.04	11
0.45	0.04	9	0.04	8
0.68	0.05	8	0.06	8
0.79	0.05	7	0.06	7
0.97	0.06	6	0.09	9
1.03	0.07	6	0.07	7

with a 2 % reading plus 2 % full scale uncertainty and maximum range of 1 dm^3/s. A type T thermocouple (Salvi Casagrande) is used to measure the air flow temperature. In this study, the CH_4 flow rate varies from 18.6 cm^3/s to 107.2 cm^3/s and the total volumetric flow rate varies from 441.1 cm^3/s to 1146.1 $\pm$ 69.8 cm^3/s, thus leading to large variations of equivalence ratio, between 0.39 and 1.03.

Considering flow measurement equipment uncertainties, the corresponding equivalence ratio uncertainty is calculated as follows [25]:

$$\frac{U_\phi^2}{\phi^2} = \left(\frac{V_f}{\phi}\frac{\partial\phi}{\partial V_f}\right)^2 \left(\frac{U_{V_f}}{V_f}\right)^2 + \left(\frac{V_a}{\phi}\frac{\partial\phi}{\partial V_a}\right)^2 \left(\frac{U_{V_a}}{V_a}\right)^2, \tag{8}$$

where ϕ is the equivalence ratio, V_f and V_a are measured fuel and air volume flow rates respectively and U_ϕ, and U_{V_f}, U_{V_a}, are the uncertainties associated with ϕ, V_f and V_a. Table 2 summarizes some representative equivalence ratios calculated with the measured air and methane flow rates and the corresponding absolute and relative uncertainties for the swirlers studied. This table allows to verify that the maximum equivalence ratio uncertainty is 11 %. The total flow rate uncertainty – not shown here for the sake of brevity –is determined in a similar fashion, and is found to lie between 6 % and 11 % for the larger and smaller flow rates, respectively. As it will be seen below, these values allow to discriminate the boundaries between the observed flame regimes

2.4 Flame imaging

In order to characterize the overall flame topologies, time-integrated chemiluminescence images of the combustion process have been obtained by using the Canon EOS Rebel T5 camera, equipped with a 58 mm diameter lens, without filters. All images presented in this study used $f-36$ aperture and exposure time of 500 ms.

A LaVision Imager Intense CCD (Charge Coupled Device) camera has been used to record flame images with an exposure time of 4 ms and $f-8$ aperture. Furthermore, a LaVision image intensifier IRO (Intensified relay-optics), equipped with a 310 nm filter, 100 % gain and gate of 100 ms has

been used. These chemiluminescence images are classically associated with the OH* radicals and, thus to the premixed flame front.

The OH* images have been deconvoluted by employing an Abel inversion technique which uses a Fourier-based algorithm [17,18]. The inversion process transforms the images obtained along the line of sight into a cross-sectional representation, assuming axial symmetry. For a given image, its center is first determined, then the deconvolution of the left and right positions is performed. In this study, 16 modes of the Fourier expansion have been used. One should note that this inversion technique is valid when axial symmetry hypothesis may hold, which is evidently not the case of the present square cross section combustion chamber. Nevertheless, the Abel-inverted OH* images are used to roughly evidence the location and shape of the average flame front.

3 Results and discussion

In this section, the flame topologies observed for each specific operating condition are first presented. The adopted topology classification follows that proposed elsewhere [20], since it is possibly the one that most closely describes the observed phenomena. The corresponding stability maps of the combustion for this experimental setup are then discussed.

3.1 Flame topologies

Three direct photos of confined flames at different combustion regimes, obtained using the SW08 swirler, are shown in Fig. 4. The swirl number computed with Eq. (7) is $S = 1.4$. All pictures have been taken with a fixed air flow rate of 1039 cm^3/s, whereas the methane varies from 83 to 111 cm^3/s. These pictures allow to verify that the flame stabilizes in three different shapes: Recirculating Zone (RZ), V and Tornado, from left to right. The images on the second row show deconvoluted OH* fields of the average flames, obtained through the use of the Abel inversion [21]. Again, each image has been obtained in the different stable regions (RZ, V and Tornado).

In Fig. 4(a) it may be assumed that a recirculating zone exists at the corner of the combustion chamber, given the structure of the flow [20,9]. Such recirculating zone flames, known as flame type IV, are observed for richer fuel/air mixtures and exhibit an important interaction with the combustion chamber walls. Indeed, this figure shows that the regions with highest luminous intensity are located along the walls of the combustion chamber.

The center picture, Fig. 4(b), presents a slightly different behavior: the flame is anchored at the swirler bluff-body only. It exhibits a V-shape – known as flame type III – and it is possible to verify that the regions with highest OH* luminous intensity are also located along the walls of the confinement, so that the flame presents a strong interaction with the walls, as is the case of flame type IV. At the used flow rates, this V-shape is found to occur for moderate equivalence ratio mixture compositions.

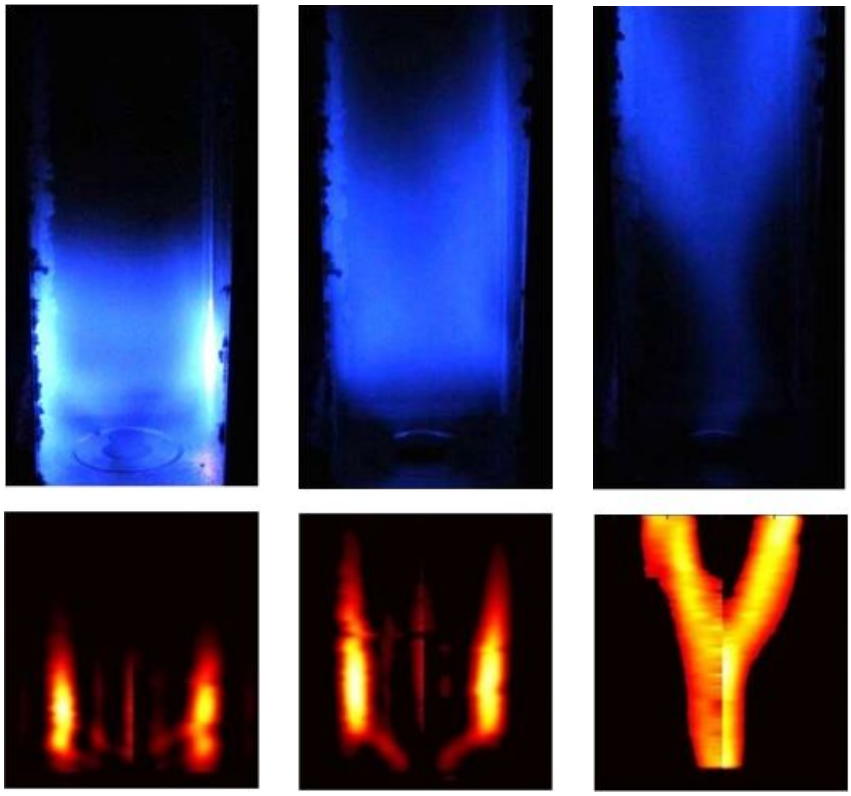

(a) $\phi = 1.12$, $\dot{\forall} = 1150\ \mathrm{cm}^3/\mathrm{s}$ (b) $\phi = 0.95$, $\dot{\forall} = 1133\ \mathrm{cm}^3/\mathrm{s}$ (c) $\phi = 0.84$, $\dot{\forall} = 1122\ \mathrm{cm}^3/\mathrm{s}$

Fig. 4 Flame topologies for different equivalence ratios (ϕ) and mixture flow rate ($\dot{\forall}$), SW08: direct photos (top), deconvoluted OH* images (bottom).

The rightmost image, Fig. 4(c), shows a flame that is found close to the blow-off limit. It has a tornado shape and does not interact with the walls, and is also known as flame type I. Analyzing the Abel-inverted image of the tornado flame, it is possible to conclude that the flame is uncoupled from the swirler and there is a flame surface bifurcation, which is associated to a higher concentration of OH* at the lateral part of the combustion chamber. It is important to highlight that there is a flame instability zone between each stable flame regimes shown, which will be discussed in section 3.2.

The observed flame topologies are controlled by the mixture composition, flow rate and swirl number. Changes in the flame shape are related with the equivalence ratio of the mixture and to acoustic instabilities [20], which suggest that:

– Shape and macro structure of the flame are related to the equivalence ratio of the mixture (when Re is constant) and significant changes are observed when critical values of fuel concentration are crossed;

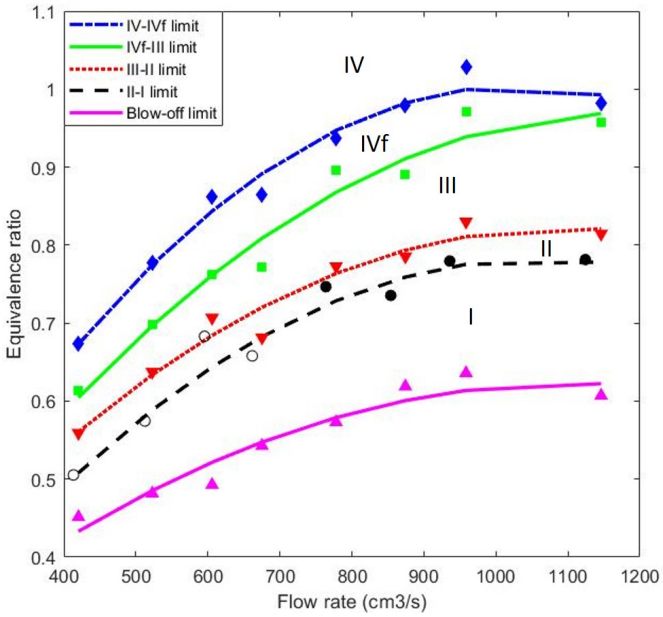

Fig. 5 Operation Regime diagram, S=1.4 - IV Stability: RZ flame, IVf Instability, III Stability: V flame, II Instability, I Stability: tornado flame. Flame blow-off occurs at the lowermost line.

- The velocity of the flow varies as the equivalence ratio changes, in other words, there is an exclusive flow associated with each flame shape;
- When the equivalence ratio increases, the burning zone becomes shorter and tends to stay closer to the swirler.

Lastly, it is important to recall that premixed flames exert a huge impact on the flow dynamics, due to the volumetric expansion along the flow path.

3.2 Operation regimes diagram

The results obtained with swirlers SW08a and SW08b are compared. To this end, the same operating conditions have been considered.

Figures 5 and 6 give diagrams where the boundaries between the combustion regimes (flame topologies) are plotted for the the swirler whose bluff-body height is $h_i = 3$ mm (SW08a) and for the one whose bluff-body height is the same as the swirler surface, $h_i = 0$ (SW08b), respectively. These diagrams shows the regimes boundaries as a function of the mixture flow rate and fuel/air equivalence ratio.

The tests have been carried out by fixing the air flow rate and progressively decreasing the methane flow rate. The air flow rates studied range from 393 to 1039 cm^3/s. In this figure, the experimentally determined regime borders are given by the symbols, each symbol corresponding to a particular regime

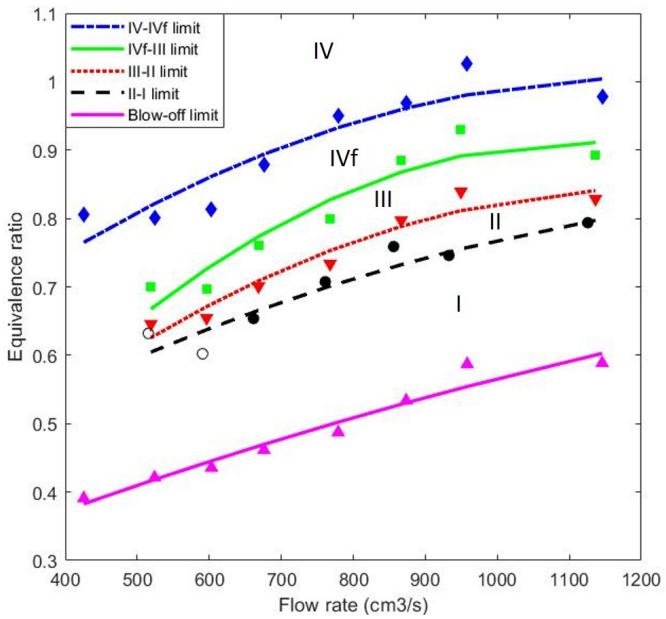

Fig. 6 Operation Regime diagram, S=0.9 - IV Stability: RZ flame, IVf Instability, III Stability: V flame, II Instability, I Stability: tornado flame. Flame blow-off occurs at the lowermost line.

border. It is important to highlight that the limits between each regime have been defined visually, and repeatedly observed to occur at the depicted symbols positions. The lines corresponding to the least squares fits of these regimes borders are also given.

Six distinct regimes have been identified, following the literature [20]. The three stable ones have been presented in the previous section. The results shown in Fig. 5 will be discussed starting from a high equivalence ratio value and progressively decreasing its value. In regime IV, the flame is stabilized at the RZ, as shown in Fig. 4(a). Upon decreasing the equivalence ratio, when the boundary is reached, the flame goes through an instability zone, IVf, where it flickers and presents a distinct acoustic tone. This seems to occur because of the intermittent flame presence at the recirculation [20]. Once the border between regions IVf and III is crossed, the flame is again stable and a corresponding representative average flame picture in this may be seen in Fig. 4(b). Indeed, the flame presents a V-shape until it reaches another instability border and moves to regime II. This regime presents a particular characteristic behavior: for small flows rates, extinction occurs – which is represented by open symbols. However, for larger flows rates – represented by solid symbols – combustion instability is observed. This second type of instability seems to be related to a large-scale, lower frequency pulsations of the combustion chamber. Further decreasing the equivalence ratio leads to regime I, which corresponding flame structure can be observed in Fig. 4(c). By decreasing the equivalence ratio the

blow-off limit is reached, which means that, at the region below the lowermost border, there is no flame within the combustor.

The swirl number computed with Eq. (7) for the swirler whose bluff-body height is the same as the swirler surface is $S = 0.9$. Concerning now SW08, for which $S = 1.4$, the stability zones IV and III are wider when compared to the swirler whose bluff-body height is the same as the swirler surface. However, for the stable regime I, the stability range is larger when $S = 0.9$, in which case the blow-off occurs at a smaller equivalence ratio. When $S = 0.9$ the boundaries are shifted downward, which means that it is possible to achieve the same regime with smaller equivalence ratio, and thus using less fuel. It should be noted that stable the flame regimes are not altered by the swirl number. However, the position of the diagram (flow rate $\times$ equivalence ratio) where each regime is observed varies, as seen above.

Recently, several studies have attempted to unveil the underlying mechanisms that control the separation between those different combustion regimes. The role of the combustor length and H_2 addition on the onset frequencies of the thermo-acoustic instabilities characteristic frequencies has been determined experimentally [23]. Even though changing the combustor length has not been attempted here, such a characteristic frequency analysis will be the subject of future work. It has been demonstrated that the boundary between regions III and IV is controlled by the flow bulk velocity and that the flame Strouhal number at the outer recirculation zone is Reynolds number independent [22]. The role of the computed premixed flame extinction strain rate on the outer recirculation zone flame frequency has also been established. Since similar regimes have been observed here, it could be anticipated that a similar scaling hold, which is currently under scrutiny. It has also been determined that, at a given equivalence ratio, the lifted flame leading edge position is independent of: (i) the ratio between the flow bulk velocity and the premixed flame speed and (ii) the adiabatic flame temperature of the combustible mixture [13]. Such a verification of independence could also have been performed here, in order to evidence the possible influence on the flame blow-off boundary displacement observed.

4 Conclusion and perspectives

The present work allowed to develop a novel radial swirler geometry featuring a central bluff-body enabling to control the swirl number by changing the bluff-body height only. A first characterization of different combustion regime/flame topologies was also performed. With these results, it was possible to identify the stability boundaries as a function of fuel and air flow rates for two swirlers having different swirl numbers. In addition, identical combustion regimes have been observed for those two swirlers, which are analogous to those found in the literature, and that involve both stable or unstable combustion.

In summary, the swirl number has been shown to influence the boundary between those combustion regimes. Indeed, the larger swirl number studied,

$S = 1.4$, led to a larger extend of stable regime III, which is a regime of practical relevance to gas turbines. However, the blow-off limit for such a swirler occurs for a larger value of equivalence ratio, which is not interesting to propulsion applications.

It should be noted that further work was recently developed on this subject [14], where a characterization of flame surface density by means of planar laser induced fluorescence of the OH radical (OH-PLIF) has been performed. The endeavor of the paper is to characterize the influence of different radial swirler configurations on the boundaries between the observed combustion regimes. In the future, the combustion chamber used will also be adapted to burn gaseous ethanol/butanol/air mixtures, thus allowing to investigate the corresponding combustion regimes changes. Combined OH-PLIF and particle imaging velocimetry measurements [3,19] should also be performed so as to unveil the detailed turbulence-chemistry interactions controlling each regime.

Acknowledgements This work was supported by PUC-Rio and Laboratoire EM2C CNRS, CentraleSupelec (France). L.F. Figueira da Silva was on leave from the Institut Prime (CNRS, France), L.C. Piton and G.S. Nobrega had scholarships from CNPq (Brazil), processes 103200/2018-5 and 372367/2017-8, respectively. The authors also gratefully acknowledge the support for the present research provided by Conselho Nacional de Desenvolvimento Científico e Tecnológico, CNPq, under the Research Grants No. 306069/2015-6 and 403904/2016-1.

References

1. Amato, A., Hudak, B., D'Carlo, P., Noble, D., Scarborough, D., Seitzman, J., Lieuwen, T.: Methane oxycombustion for low CO_2 cycles: Blowoff measurements and analysis. Journal of Engineering for Gas Turbines and Power **133**, 1–9 (2011)
2. Bourgouin, J., Moeck, J., Durox, D., Schuller, T., Candel, S.: Sensitivity of swirling flows to small changes in the swirler geometry. Comptes Rendus Mecanique **341**, 211–219 (2013)
3. Caetano, N.R., Figueira da Silva, L.F.: A comparative experimental study of turbulent non premixed flames stabilized by a bluff-body burner. Experimental Thermal and Fluid Science **63**, 20 – 33 (2015)
4. Candel, S., Durox, D., Schuller, T., Bourgouin, J., Moeck, J.: Dynamics of swirling flames. Annual Review of Fluid Mechanics **46**, 147–173 (2014)
5. Cavaliere, D.E., Kariuki, J., Mastorakos, E., Cavaliere, D.E., Kariuki, J., Mastorakos, E.: A comparison of the blow-off behaviour of swirl-stabilized premixed, non-premixed and spray flames. Flow, Turbulence and Combustion **91**, 347–372 (2013)
6. Chterev, I., Foley, C., Foti, D., Kostka, S., Caswell, A., Jiang, N., Lynch, A., Noble, D., Menon, S., Seitzman, J., Lieuwen, T.: Flame and flow topologies in an annular swirling flow. Combustion Science and Technology **186**, 1041–1074 (2014)
7. Durox, D., Moeck, J., Bourgouin, J., Morenton, P., Viallon, M., Schulle, T., Candel, S.: Flame dynamics of a variable swirl number system and instability control. Combustion and Flame **160**, 1729–1742 (2013)
8. Galley, D., Ducruix, S., Lacas, F., Veynante, D.: Mixing and stabilization study of a partially premixed swirling flame using laser induced fluorescence. Combustion and Flame **158**, 155–171 (2011)
9. Guiberti, T., Durox, D., Zimmer, L., Schuller, T.: Analysis of topology transitions of swirl flames interacting with the combustor side wall. Combustion and Flame **162**(11), 4342–4357 (2015)

10. Huang, Y., Yang, V.: Dynamics and stability of lean-premixed swirl-stabilized combustion. Progress in Energy and Combustion Science **35**, 293–364 (2009)
11. Jerzak, W., Ku, M.: Experimental study of impact of swirl number as well as oxygen and carbon dioxide content in natural gas combustion air on flame flashback and blow-off. Journal of Natural Gas Science and Engineering **29**, 46–54 (2016)
12. Jourdaine, P., Mirat, C., Caudal, J., Lo, A., Schuller, T.: A comparison between the stabilization of premixed swirling CO_2- diluted methane oxy-flames and methane/air flames. Fuel **201**, 156–164 (2017)
13. Jourdaine, P., Mirat, C., Caudal, J., Lo, A., Schuller, T.: A comparison between the stabilization of premixed swirling co2-diluted methane oxy-flames and methane/air flames. Fuel **201**, 156 – 164 (2017)
14. Nobrega, G.S., Piton, L.C., Figueira da Silva, L.F., Scouflaire, P., Darabiha, N.: Experimental study of the effect of the swirl number on premixed combustion regimes and flame topologies. In: 11th Mediterranean Combustion Symposium (MCS 2019). Tenerife, Spain (2019)
15. Nogenmyr, K., Cao, H., C.K., C., Cheng, R.K.: Effects of confinement on premixed turbulent swirling flame using large eddy simulation. Combustion Theory and Modelling **17**, 1003–1019 (2013)
16. Orbay, R., Nogenmyr, K., Klingmann, J., Bai, X.: Swirling turbulent flows in a combustion chamber with and without heat release. Fuel **104**, 133–146 (2013)
17. Pretzier, G.A.: A new method for numerical abel-inversionl. Zeitschrift für Naturforschung **46**, 639–641 (1991)
18. Pretzier, G.A., Jäger, H., Neger, T., Philipp, H., Woisetschläger, J.: Comparison of different methods of abel inversion using computer simulated and experimental side-on data. Zeitschrift für Naturforschung **47a**, 639–641 (1992)
19. Roque Ccacya, A.O., Figueira da Silva, L.F.: Characterization of multi-jet turbulent flames in cross flow using stereo-piv and oh-plif. Fire Safety Journal **78**, 44 – 54 (2015)
20. Shanbhogue, S., Sanusi, Y., Taamallah, S., Habib, M., Mokheimer, E., Ghoniem, A.: Flame macrostructures, combustion instability and extinction strain scaling in swirl-stabilized premixed CH_4/H_2 combustion. Combustion and Flame **163**, 494–507 (2016)
21. Figueira da Silva, L.F., Mergulhão, S., Piton, L.C., Scouflaire, P., Darabiha, N.: Experimental study of a lean premixed turbulent swirling flame stabilization. In: 24th ABCM International Congress of Mechanical Engineering. Curitiba, Brazil (2017)
22. Taamallah, S., Chakroun, N.W., Watanabe, H., Shanbhogue, S.J., Ghoniem, A.F.: On the characteristic flow and flame times for scaling oxy and air flame stabilization modes in premixed swirl combustion. Proceedings of the Combustion Institute **36**(3), 3799 – 3807 (2017)
23. Taamallah, S., LaBry, Z.A., Shanbhogue, S.J., Ghoniem, A.F.: Thermo-acoustic instabilities in lean premixed swirl-stabilized combustion and their link to acoustically coupled and decoupled flame macrostructures. Proceedings of the Combustion Institute **35**(3), 3273 – 3282 (2015)
24. Tong, Y., Li, M., Jens, K.: Influence of combustor geometry on swirl stabilized premixed methane-air flame. In: Proceedings of ASME Turbo Expo 2016: Turbomachinery Technical Conference and Exposition, pp. 1–10 (2016)
25. Tripathi, M.M., Srinivasan, K.K., Krishnan, S.R., Yueh, F.Y., Singh, J.P.: A comparison of multivariate libs and chemiluminescence-based localequivalence ratio measurements in premixed atmospheric methaneair flames. Fuel **106**, 318 – 326 (2013)
26. Watanabe, H., Shanbhogue, S.J., Taamallah, S., Chakroun, N.W., Ghoniem, A.F.: The structure of swirl-stabilized turbulent premixed CH_4/air and $CH_4/O_2/CO_2$ flames and mechanisms of intense burning of oxy-flames. Combustion and Flame **174**, 111–119 (2016)